

## Constraining Land Surface and Atmospheric Parameters of a Locally Coupled Model Using Observational Data

YUQIONG LIU, HOSHIN V. GUPTA, SOROOSH SOROOSHIAN,\* LUIS A. BASTIDAS,<sup>+</sup> AND WILLIAM J. SHUTTLEWORTH

*Department of Hydrology and Water Resources, The University of Arizona, Tucson, Arizona*

(Manuscript received 4 May 2004, in final form 9 September 2004)

### ABSTRACT

In coupled land surface–atmosphere modeling, the possibility and benefits of constraining model parameters using observational data bear investigation. Using the locally coupled NCAR Single-column Community Climate Model (NCAR SCCM), this study demonstrates some feasible, effective approaches to constrain parameter estimates for coupled land–atmosphere models and explores the effects of including both land surface and atmospheric parameters and fluxes/variables in the parameter estimation process, as well as the value of conducting the process in a stepwise manner. The results indicate that the use of both land surface and atmospheric flux variables to construct error criteria can lead to better-constrained parameter sets. The model with “optimal” parameters generally performs better than when a priori parameters are used, especially when some atmospheric parameters are included in the parameter estimation process. The overall conclusion is that, to achieve balanced, reasonable model performance on all variables, it is desirable to optimize both land surface and atmospheric parameters and use both land surface and atmospheric fluxes/variables for error criteria in the optimization process. The results also show that, for a coupled land–atmosphere model, there are potential advantages to using a stepwise procedure in which the land surface parameters are first identified in offline mode, after which the atmospheric parameters are determined in coupled mode. This stepwise scheme appears to provide comparable solutions to a fully coupled approach, but with considerably reduced computational time. The trade-off in the ability of a model to satisfactorily simulate different processes simultaneously, as observed in most multicriteria studies, is most evident for sensible heat and precipitation in this study for the NCAR SCCM.

### 1. Introduction

The ever-growing large family of land surface schemes (e.g., Sellers et al. 1986; Dickinson et al. 1986, 1993) has initiated a suite of intercomparison and evaluation projects, such as the Project of Intercomparison of Land Surface Parameterization Schemes (PILPS; Henderson-Sellers et al. 1995) and the Global Soil Wetness Project (GSWP; Dirmeyer et al. 1999). These offline (or stand-alone) studies allow the evaluation of performances of land surface schemes without the complications associated with the errors in the at-

mospheric components of global climate models. More recently, with the increasing availability of global observations from ground- and space-based systems, offline land surface modeling studies have matured into interesting projects such as the Global Land Data Assimilation System (GLDAS; Rodell et al. 2004) and the North American Land Data Assimilation System (NLDAS; Cosgrove et al. 2003), which are capable of producing reliable, high-resolution estimates of land surface water and energy fields to facilitate predicting weather and climate. Regardless all of these benefits, offline studies prevent the investigation of the interactions and feedbacks between the land surface and the atmosphere, leaving unanswered questions regarding the relevance of these offline applications to the fully coupled land–atmosphere system and the suitability of the land surface schemes validated in an offline mode to operational numerical weather forecasting and climate prediction models. A few studies have suggested that offline experiments can lead to misleading results and thus do not provide reliable information on the performance of a land surface scheme in global climate models (e.g., Koster and Eagleson 1990; Dolman and Gregory 1992; Pitman et al. 1993; among others).

\* Current affiliation: Department of Civil and Environmental Engineering, University of California, Irvine, Irvine, California.

<sup>+</sup> Current affiliation: Department of Civil and Environmental Engineering, Utah State University, Logan, Utah.

*Corresponding author address:* Yuqiong Liu, SAHRA—An NFC Center for Semi-Arid Hydrology and Riparian Areas, The University of Arizona, Marshall Building, Room 535, 845 N. Park Avenue, P.O. Box 210158-B, Tucson, AZ 85721-0158.  
E-mail: yqliu@hwr.arizona.edu

As the performance of a land surface model is inevitably affected by the choice of model parameters, similar questions also arise regarding how feedbacks within the coupled system affect the identification of “optimal” model parameters and whether parameter values estimated via offline methods are suitable to the coupled land–atmosphere system. Sen et al. (2001) reported statistically significant changes in the simulated temperature and precipitation fields of a global climate model when “optimal” values of some vegetation parameters derived from an offline calibration of the land surface model were applied, indicating that the choice of surface parameter values can significantly influence the surface climate simulated by a global climate model. It is, then, of interest to examine whether the parameter estimations for a coupled system are considerably affected by model-generated surface climate. Up to the present, little or no attention has been paid to the estimation of parameters of land–atmosphere models in a coupled mode, where the effects of land–atmosphere interactions on the identification of optimal parameters can be taken into account, and calibration can be performed on both land and atmospheric parameters. Further, as indicated by Gupta and Sorooshian (1985), the quantity and quality of data play a critical role in determining the success of the parameter estimation procedure, and the informativeness of the data is far more important than the length and amount used for parameter estimation. In the coupled environment, data related to both land surface and atmospheric fluxes/variables can be used to facilitate more effective extraction of information from the observations to constrain the estimation of model parameters.

Over the past two decades, the issue of model calibration has received substantial attention within the hydrological and land surface modeling community. For example, Sellers et al. (1989) calibrated the Simple Biosphere Model (SiB; Sellers et al. 1986) to five 2-week periods of field data via manual adjustment of nine model parameters. More recently, Lettenmaier et al. (1996) reported at the PILPS-2c workshop that subjective manual calibration of some model parameters led to significantly improved model performances. Substantial research has also been devoted to the development of automatic methods, such as the shuffled complex evolution algorithm (SCE-UA; Duan et al. 1992) and the multiobjective complex evolution algorithm (MOCOM-UA; Yapo et al. 1998). Sorooshian et al. (1993) employed the global optimization algorithm SCE-UA to successfully calibrate the Sacramento Soil Moisture Accounting model (SAC-SMA; Burnash et al. 1973), while Gupta et al. (1998, 1999) and Xia et al. (2002) used MOCOM-UA to conduct multiobjective calibrations for the SAC-SMA, the Biosphere–Atmosphere Transfer Scheme (BATS 1e; Dickinson et al. 1993), and the Chameleon Surface Model (CHASM; Desborough 1999), respectively. These calibration stud-

ies, although all conducted in an offline mode, can provide valuable guidance for parameter estimations in a coupled system as is performed in this study.

In light of the current infeasibility of optimizing all the parameters directly within a fully coupled global model, this study investigates the application of a multicriteria parameter estimation method to the locally coupled environment of a single-column model (SCM), with attention given to the parameters and fluxes/variables of both the land and atmospheric components of the model. The primary goal is to explore the feasibility and effects of performing model calibration in a locally coupled environment, and the manner in which different types of observational data can be used to constrain parameter and simulation uncertainties. In section 2, the locally coupled SCM and land surface model used in this study are introduced briefly, along with a brief description of the data used to drive and evaluate the models. The parameter estimation procedure is presented in section 3. Analyses of the results from a set of single-step coupled optimization cases follow in section 4. The results from three additional stepwise cases are presented and compared in section 5, while section 6 is devoted to discussions and concluding remarks.

## 2. Models and data

The locally coupled National Center for Atmospheric Research Single-column Community Climate Model (NCAR SCCM, hereinafter referred to as the SCCM), and the offline version of the land surface model coupled to the SCCM, the NCAR Land Surface Model (NCAR LSM, hereinafter referred to as the LSM), were used in this study.

### a. The LSM

The LSM is a one-dimensional, time-dependent model describing the momentum, energy, water, and CO<sub>2</sub> flux exchanges and interactions between land surfaces and the atmosphere (Bonan 1996). The model allows for multiple surface types in a single grid cell, accounting for ecological differences among 12 different vegetation types, and takes into account the optical, thermal, and hydraulic differences among 8 different soil types with different combinations of percentages of sand, silt, and clay. The atmospheric forcing terms required to drive the model include incident direct and diffuse solar radiation, incident longwave radiation, convective and large-scale precipitation, specific humidity, temperature, pressure, wind, and reference height. When driven by these forcing terms, which can be generated by an atmospheric model or specified from observations, the LSM calculates diffuse and direct surface albedos, zonal and meridional momentum fluxes, constituent fluxes (H<sub>2</sub>O and CO<sub>2</sub>), surface-

emitted longwave radiation, surface sensible and latent heat fluxes, soil and vegetation temperatures, and soil moisture contents. For details of the model physics, interested readers are referred to Bonan (1996), in which a comprehensive description about the model is provided.

The LSM has been used in a number of ecological, hydrological, and atmospheric studies. For example, Bonan et al. (1997) and Lynch et al. (1999) compared the LSM-simulated surface fluxes to the observations for the boreal forest sites in Canada and the tundra ecosystems in Alaska, respectively; Lynch et al. (2001) used a multivariate reduced form model to investigate the sensitivity of the LSM to perturbations in climate forcing. Other LSM-related studies include Bonan (1995a) and Craig et al. (1998), in which the LSM was used to investigate the land-atmosphere CO<sub>2</sub> exchanges; Bonan (1995b), in which the sensitivity of a GCM simulation to the inclusion of inland water surfaces was explored; and Bonan (1997, 1999), in which the effects of land cover changes on the climate of the United States were studied.

In this study, the parameterization of canopy evapotranspiration of the LSM was slightly adjusted to allow for more reasonable simulations of latent and sensible heat fluxes. In the original LSM, the canopy evapotranspiration is calculated based only on energy availability, with no constraint of water availability, resulting in unrealistic surface energy partitions. For details, interested readers are referred to Liu et al. (2003), where in an effective parameterization adjustment was made with a maximum canopy evaporation constraint, leading to significantly improved model performances.

### b. The SCCM

The SCCM is a single-grid column model developed from the NCAR global climate model Community Climate Model Version 3 (CCM3). The physical parameterizations in the SCCM, such as those of radiation, clouds, deep and shallow convection, large-scale condensation, and boundary layer processes, are the same as those in the CCM3. Kiehl et al. (1996) provided more details on the physical parameterization of the CCM3. The advantage of using the SCCM instead of the fully coupled CCM3 is that single-column model applications can avoid huge computational expenses and the difficulty of separating the effects of specific parameterizations from those of other complicated interdependent processes (Xu and Arakawa 1992; Randall et al. 1996). The SCCM, however, lacks the horizontal feedbacks available in the more complicated three-dimensional CCM3, making it necessary to prescribe the horizontal advective tendencies using observations or analysis data. Interested readers may refer to Hack et al. (1999) and Randall and Cripe (1999) for information about specifying the effects of neighboring columns in the SCCM.

### c. Data

In this study, both the offline LSM and the locally coupled SCCM were driven and evaluated using an intensive operational period (IOP) dataset from the southern Great Plains (SGP; <http://www.arm.gov/docs/sites/sgp/sgp.html>) Clouds and Radiation Testbed (CART) of the Atmospheric Radiation Measurement (ARM; [www.arm.gov](http://www.arm.gov)) Program. The data have previously been subjected to a constrained variational analysis (Zhang and Lin 1997; Zhang et al. 2001), with all relevant variables representing areal means over an SCM domain enclosed by 12 facilities centered around a central facility (36.61°N, 97.49°W; 320 m above sea level). This IOP dataset extends for 17.5 days from 0530 UTC 18 July 1995 (0030 local time) to 1730 UTC 4 August 1995 (1230 local time) and represents various summer weather conditions, including several intensive precipitation periods.

The IOP dataset contains both single-level variables, such as surface heat fluxes, ground temperature, surface net downward radiation, precipitation, surface pressure, and surface winds, and multilayer fields, such as temperature, specific humidity, winds, vertical velocity, and horizontal and vertical advective tendencies for temperature and specific humidity. To be consistent with the default time step length (20 min) of the SCCM and the LSM, all the variables available in this IOP dataset were interpolated<sup>1</sup> at 20-min intervals based on the original 3-h observational data using cubic spline interpolation.

## 3. Parameter estimation procedure

The purpose of parameter estimation is to constrain the space of model parameters to those exhibiting behaviors that are consistent with the available observational data. This problem can be presented in the form of a mathematical optimization problem where one or more model responses are optimized to become consistent with their corresponding observations. Duan et al. (1992) presented an effective global optimization scheme, the SCE-UA, for single-criterion calibration problems, while Yapo et al. (1998) introduced the MOCOM-UA, which produces a set of mutually nondominated Pareto solutions (Goldberg 1989) or parameter sets for multicriteria calibration problems.

Besides the MOCOM-UA, distinct Pareto solutions can also be obtained sequentially using classical multi-objective optimization techniques, such as the weighting method which transforms a multiobjective optimization problem into an equivalent single-objective optimization problem by allocating different weights to the multiple objectives. In conjunction with the weighting method, the single-objective algorithm SCE-UA

<sup>1</sup> Done by John Pedretti as indicated in the NetCDF data file.

can be used to solve multiobjective model calibration problems as described in Gupta et al. (1998). To illustrate the weighting method, we consider a multiobjective optimization problem having  $n$  objectives  $\{f_j(\theta), j = 1, \dots, n\}$  to be minimized simultaneously, where  $\theta$  represents the parameter set to be optimized. By allocating a weight to each of the  $n$  objectives, the multiobjective optimization problem can be converted into a single-objective optimization problem as follows:

$$\text{Minimize } F(\theta) = \sum_{j=1}^n w_j f_j(\theta) \text{ subject to } \theta \in \Theta, \quad (1)$$

where  $w_j$  ( $j = 1, \dots, n$ ) are the weights and  $w_1 + w_2 + \dots + w_n = 1$ , and  $\Theta$  is the physically feasible parameter space;  $F(\theta)$  is a scalar objective function. This problem is easily solved using standard single-objective optimization algorithms such as the SCE-UA. An approximate Pareto set can be obtained by running the optimization algorithm using different weight combinations for the  $n$  objectives. For example, by allocating equal weights  $\{w_j = 1/n, j = 1, \dots, n\}$  to the objectives, a compromise solution (i.e., the midpoint of the Pareto set) can be obtained. Although it is relatively time consuming to approximate the entire Pareto space using this weighting method, some studies (e.g., Yan and Haan 1991; Leavesley et al. 1983) have reported that it can achieve better model performance than pure single-objective optimization algorithms.

In practice, because the objectives to be minimized are usually in different units, the weighting method presented above cannot be applied directly. For example, for a land surface model, it is usually necessary that at least one surface heat flux (such as latent heat) and one state variable (such as ground temperature) be simultaneously optimized to achieve desirable results (Gupta et al. 1999). In this case, some transformation must be performed on the different objectives to place them in commensurable units (or make them unitless) so that the objectives can be weighted and summed up to create a single-objective optimization problem. One simple and common approach is to normalize the objectives within reasonable lower and upper bounds. The optimization problem can then be stated as

$$\text{Minimize } F(\theta) = \sum_{j=1}^n w_j f'_j(\theta) \text{ subject to } \theta \in \Theta, \quad (2)$$

$$\text{with } f'_j(\theta) = \frac{f_j(\theta) - f_j^{\min}}{f_j^{\max} - f_j^{\min}}, \quad (3)$$

where  $f_j^{\min}$  and  $f_j^{\max}$  are arbitrarily estimated minimum and maximum objective function values for the  $j$ th objective.

In this study, because the complicated interactions between the land surface and the atmosphere makes the multiobjective algorithm MOCOM-UA somewhat cumbersome, SCE-UA, combined with the modified

weighting method mentioned above, was used for the parameter estimation for the SCCM. SCE-UA starts with the random initial selection of a "population" of points from the feasible parameter space, and the objective function values for each point are calculated. The population is then partitioned into several complexes based on the corresponding objective function values. After evolving separately for a prescribed number of times based on the downhill simplex search algorithm, the complexes, each containing new points (offsprings), are unpacked back into a single group and the "population" is shuffled and partitioned into new complexes. The evolution and shuffling steps are repeated until a prescribed convergence criterion is satisfied. The details about the SCE-UA can be found in Duan et al. (1992). In this study, when weighting each objective using Eq. (3), the  $f^{\min}$  was set to zero and the  $f^{\max}$  was set to the corresponding objective function value computed with the a priori or "default" parameters. To save computational time, the entire Pareto front was not sought. Instead, equal weights were assigned to each objective and a Pareto ranking was performed on the final optimal solutions to identify a subset of Pareto optimal points (parameter sets) in the region of the compromise point to analyze the optimization results.

#### 4. Parameter estimation in a locally coupled mode

##### a. Case design

A locally coupled land surface-atmosphere model consists of two important components (or submodels): an atmospheric column and a land surface part. In the case of the SCCM, the two parts are coupled with an explicit time-stepping procedure: the land surface part is driven by the calculated state of the atmosphere (precipitation, shortwave and longwave downward radiation, air temperature, specific humidity, surface pressure, zonal and meridional winds); the atmospheric part is then updated with surface energy (latent and sensible heat), constituents ( $\text{H}_2\text{O}$  and  $\text{CO}_2$ ), momentum, and radiative fluxes computed by the land surface part. Hence, from the point of view of model parameter estimation, observations on both land surface and atmospheric fluxes/variables (such as precipitation, radiation, and air temperature) can be used to constrain the selection of parameter sets. Further, both land surface parameters ( $\{\theta\}$ ) and atmospheric parameters ( $\{\phi\}$ ) can be adjusted during the parameter estimation process.

In this study, observations on two land surface fluxes (latent heat  $\lambda E$  and sensible heat  $H$ ), a land surface state variable (ground temperature  $T_g$ ), and three atmospheric forcing variables (precipitation  $P_{cp}$ , net downward radiation at the surface  $R_{net}$ , and air temperature  $T_a$ ) were used for parameter estimation. These variables were selected based on the observations available and their expected critical importance in the land-

TABLE 1. Land surface and atmospheric parameters selected for optimization.

Parameter	Default	Lower	Upper	Description (units)	Case D <sub>3</sub>
Nine parameters associated with vegetation (vegetation type = 11, crop)					
1 ZOMVT	0.06	0.01	0.1	Momentum roughness length of vegetation (m)	{ $\theta^{def}$ } 0.09
2 ZPDVT	0.34	0.2	0.4	Displacement height (m)	0.30
3 RHOL2	0.58	0.35	0.58	Leaf reflectance in NIR	0.38
4 TAUL2	0.25	0.1	0.25	Leaf transmittance in NIR	0.14
5 XL	-0.3	-0.4	0.6	Leaf orientation index	0.45
6 CH2OP	0.1	0.05	0.5	Maximum intercepted water per unit leaf area index (lai) + stem area index (sai) (mm)	0.07
7 HVT	0.5	0.35	1	Top of canopy (m)	0.59
8 AVCMX	2.4	1	3	Temperature sensitivity parameter for carboxylation	1.00
9 COVER	0.85	0.3	0.98	Vegetation cover fraction (%)	0.55
12 parameters associated with soil (soil color = 8)					
10 RLSOI	0.05	0.004	0.1	Roughness length of soil (m)	0.028
11 WATSAT	0.435	0.33	0.66	Volumetric soil water content at saturation (porosity)	0.643
12 HKSAT	4.19E-03	1.00E-05	0.1	Hydraulic conductivity at saturation (mm H <sub>2</sub> O s <sup>-1</sup> )	0.056
13 SMPSAT	-207	-750	-30	Soil matrix potential at saturation (mm)	-345
14 BCH	5.772	3	10	Clapp and Hornberger "b"	6.01
15 WATDRY	0.122	0.02	0.3	Soil water content when evapotranspiration stops	0.06
16 WATOPT	0.331	0.2	0.8	Optimal soil water content for evapotranspiration	0.583
17 TKDRY	0.15	0.1	3	Thermal conductivity, dry soil (W m <sup>-1</sup> K <sup>-1</sup> )	0.102
18 CSOL	2.20E+06	2.00E+05	5.00E+06	Specific heat capacity, soil solids (J m <sup>-3</sup> K <sup>-1</sup> )	1.1E+06
19 ALBSAT1	0.05	0.05	0.12	Saturated soil albedo in visible (VIS)	0.116
20 ALBSAT2	0.1	0.1	0.2	Saturated soil albedo in near-infrared (NIR)	0.132
21 DZSOI1	0.1	0.05	0.2	Thickness for the first soil layer (m)	0.196
Two initial soil moisture conditions					
22 H2OSOI1	0.3	0.01	0.4	Initial volumetric soil water content, first layer	0.182
23 H2OSOI2	0.3	0.1	0.5	Initial volumetric soil water content, second layer	0.28
Eight atmospheric parameters associated with deep convection and cloud fraction					
24 CAPELMT	70	0.01	3000	Threshold value of CAPE for deep convection (J kg <sup>-1</sup> )	{ $\phi$ } Range 1471-1630
25 TAU	7200	2400	9600	Adjustment time scale for CAPE consumption (s)	6360-6910
26 FMAX	0.0002	0.0001	0.0005	Max fractional entrainment rate of updrafts	.0004-.0005
27 ALFA	0.1	0.01	0.5	Proportionality factor for downdraft mass flux profile	0.26-0.31
28 RHMINL	0.9	0.7	0.98	Min relative humidity for low cloud formation	0.75-0.76
29 RHMINH	0.9	0.7	0.98	Min relative humidity for midlevel and high cloud formation	0.97-0.98
30 CCONV	0.035	0.01	0.06	Coefficient for calculating column convective cloud	0.012-0.016
31 RHCCN	0.1	0.05	0.3	Reduction on RHMINL for CCN rich land areas	0.29-0.30

atmosphere interface. In all cases, the root-mean-squared error (rmse) of the residuals (differences between the observed and simulated quantities at each time step) was used as the objective function. In the case of precipitation, however, the rmse was computed using the accumulative precipitation depth (millimeters) during a 6-h period (18 time steps) instead of the average instant precipitation rate (meters per second) over a single 20-min time step. Based on a previous parameter sensitivity analysis study (Liu et al. 2004), 23 land surface parameters and 8 atmospheric parameters (Table 1) were selected for optimization.

To explore different mechanisms and strategies for parameter estimation in a locally coupled environment,

a series of cases was designed. The experiments were categorized into 1) group A, in which only land surface parameters  $\{\theta\}$  were optimized, while the atmospheric parameters  $\{\phi\}$  were fixed at default values  $\{\phi^{def}\}$ ; 2) group B, in which only atmospheric parameters  $\{\phi\}$  were optimized, with  $\{\theta\}$  fixed at default values  $\{\theta^{def}\}$ ; and 3) group C, in which both land surface and atmospheric parameters were optimized simultaneously. Each group (A, B, or C) was further divided into 1) a "first" case in which only land surface fluxes/variables (including  $\lambda E$ ,  $H$ , and  $T_g$ ) were used for optimization, 2) a "second" case in which only atmospheric variables (including  $P_{cp}$ ,  $R_{net}$ , and  $T_a$ ) were used for optimization, and 3) a "third" case in which both land surface

variables ( $\lambda E$ ,  $H$ ,  $T_g$ ) and atmospheric variables ( $P_{cp}$ ,  $R_{net}$ ,  $T_a$ ) were used for optimization; the purpose was to examine the relative usefulness of the atmospheric data as compared to land surface observations for constraining parameter and simulation uncertainties. As a result, nine cases were established:  $A_1$ ,  $A_2$ ,  $A_3$ ,  $B_1$ ,  $B_2$ ,  $B_3$ ,  $C_1$ ,  $C_2$ , and  $C_3$  (Table 2). The results from each case were examined and compared in terms of the final “optimal” parameter sets, the corresponding objective function values, and the time series of the evaluation variables ( $\lambda E$ ,  $H$ ,  $T_g$ ,  $P_{cp}$ ,  $R_{net}$ , and  $T_a$ ).

### b. Optimal parameter sets

The optimal land surface parameter sets are shown in Fig. 1a for cases  $A_1$  (red),  $A_2$  (green), and  $A_3$  (blue) and in Fig. 1b for cases  $C_1$  (red),  $C_2$  (green), and  $C_3$  (blue), while the optimal atmospheric parameter sets are presented in Fig. 1c for cases  $B_1$  (red),  $B_2$  (green), and  $B_3$  (blue) and in Fig. 1d for cases  $C_1$  (red),  $C_2$  (green), and  $C_3$  (blue). In A cases and B cases, the a priori or default values were used for atmospheric and land surface parameters, respectively, and thus are not shown in these figures. Each line going from left to right across the plot corresponds to a different parameter set, with the parameters (land or atmospheric) listed on the  $x$  axes and the  $y$  axes corresponding to the parameter values normalized by the ranges between the lower and upper bounds of the parameters (Table 1). The default parameter set is also plotted in black for comparison. For each parameter estimation case, instead of picking a single representative solution to analyze the results, the Pareto set from the final members is shown. The individual points of each parameter set are connected to help visualize the constraining of parameter estimations in each case.

It is not surprising to notice from Figs. 1a–d that, because of land–atmosphere parameter interdependencies, the optimal land surface parameters estimated in the A cases and the optimal atmospheric parameters estimated in the B cases tend to be different from those obtained in the C cases. Overall, Figs. 1a–d show that,

for most of the land surface and atmospheric parameters, the optimal values estimated by the parameter estimation procedures are typically different from the default values. For example, in groups A and C, the optimal values of XL (leaf orientation index), ALBSAT1, and ALBSAT2 (soil albedos) have all converged to higher values in the parameter space compared to the default values. For the atmospheric parameters (Figs. 1c and 1d), the optimal values of rhminl (the threshold of relative humidity for low cloud formation) tend to be low compared to the default value (rhminl = 90%), while those of rhccn [the reduction on rhminl for (cloud condensation nuclei) CCN-rich land areas] tend to be high compared to the default value (rhccn = 10%). This indicates that, in the SCCM, the prescribed threshold value of relative humidity for low cloud formation over land areas (i.e., 80%) may be too high for the model to simulate the observed cloud amounts. This is consistent with the results from Somerville and Iacobellis (1999), who pointed out that ARM observations indicate that the actual maximum relative humidity when clouds are present is less than 80%, suggesting that the use of 80% as critical relative humidity for cloud formation over land areas in many GCMs may need to be reexamined. Also, the default value of the threshold of convective available potential energy (CAPE) for deep convection (CCONV) tends to be small compared to the estimates from most of the experiments.

To minimize simulation uncertainties associated with parameter uncertainties, well-constrained optimal parameter sets are desired. As shown in Figs. 1a and 1b, for the land surface parameters, all cases in groups A and C tend to provide fairly well constrained (or grouped) parameters sets. However, the parameter sets in the second and third cases (green and blue) appear to be more tightly constrained than in the first cases (red) for both A and C groups, particularly for several soil parameters, including WATSAT, HKSAT, CSOL, and ALBSAT1. This is also true for most vegetation parameters (the first nine parameters in Figs. 1a and 1b), and especially for XL (leaf orientation index). Note that the second and third cases include atmospheric variables ( $P_{cp}$ ,  $R_{net}$ , and  $T_a$ ) in the parameter estimation procedure (while the first cases include only land surface fluxes/variables), indicating the value of using observations on atmospheric variables to help constrain the values of the land surface parameters. Figure 1d shows that, in the C group, wherein both land surface and atmospheric parameters are optimized, the use of atmospheric variables as calibration criteria in  $C_2$  (green) and  $C_3$  (blue) can also help to better constrain the atmospheric parameters compared to  $C_1$ , especially for RHMINH. However, when only atmospheric parameters are optimized in the procedure (group B; Fig. 1c), it seems insufficient to use only atmospheric variables: several atmospheric parameters are poorly constrained in case  $B_2$  (green), including alfa, RHMINL, rhminh,

TABLE 2. The single-step cases.

Case	Evaluation variables	Land surface parameters ( $\theta$ )	Atmospheric parameters ( $\phi$ )
A cases	$A_1$	Optimized	Default
	$A_2$		
	$A_3$		
B cases	$B_1$	Default	Optimized
	$B_2$		
	$B_3$		
C Cases	$C_1$	Optimized	Optimized
	$C_2$		
	$C_3$		

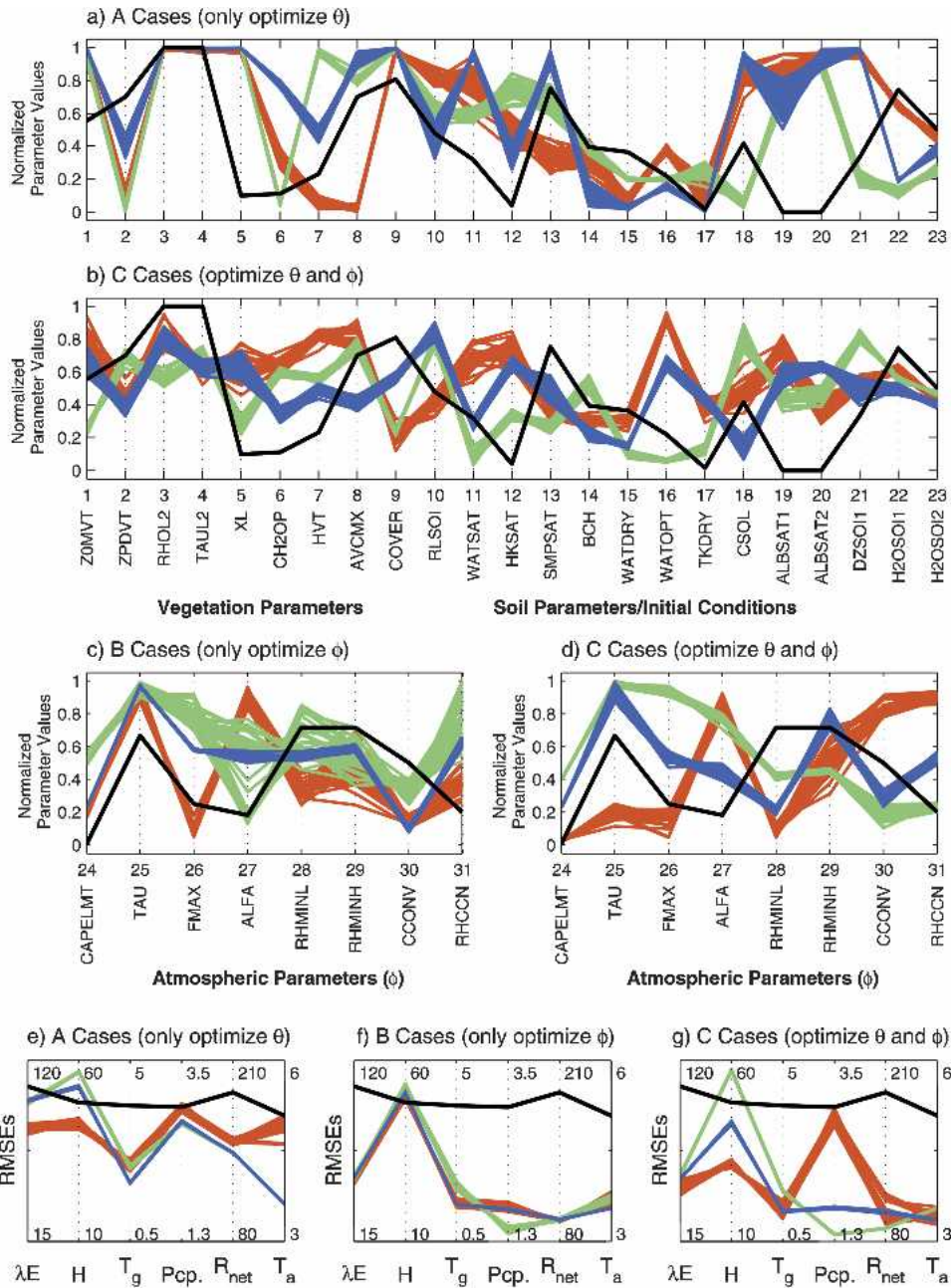


FIG. 1. Comparison of parameter estimates and final objective function values for different cases: (a) normalized land surface parameter estimates for the A cases (black = default, red =  $A_1$ , green =  $A_2$ , blue =  $A_3$ ); (b) same as (a) but for the C cases; (c) normalized atmospheric parameter estimates for the B cases (black = default, red =  $B_1$ , green =  $B_2$ , blue =  $B_3$ ); (d) same as (c) but for the C cases; (e) objective function values (rmse) for the A cases [same color code as in (a)]; (f) same as (e) but for the B cases; and (g) same as (e) but for the C cases. Values shown in the bottom and top of (e)–(g) provide the ranges used to plot the rmse.

and rhccn; these parameters, however, are better constrained in cases  $B_1$  and  $B_3$  (especially  $B_3$ ) when some land surface fluxes/variables were used. Collectively, these results support the intuitive notion that using both land surface and atmospheric fluxes/variables can help to better constrain the parameter sets, thereby re-

ducing the uncertainty associated with the parameter estimates.

### c. Objective function values

The rmse criterion was used as the objective function in this study. Shown in Figs. 1e–g are the trade-offs

between the six variables ( $\lambda E$ ,  $H$ ,  $T_g$ ,  $P_{cp}$ ,  $R_{net}$ , and  $T_a$ ) in the multicriteria space for A, B, and C cases, respectively, with the same color code as in Figs. 1a–d. The variables are listed along the  $x$  axes, while the  $y$  axes correspond to the rmses; the numbers shown at the top and bottom of each figure provide the ranges used to plot the rmses of the six variables. In these plots, each line going from left to right corresponds to a solution (i.e., a different parameter set in Figs. 1a–d). If a line representing a solution falls entirely below (above) that of a different solution, the former can be considered to be absolutely superior (inferior) to the latter from the multicriteria point of view, otherwise, if the two lines cross each other, the two corresponding solutions are considered as noninferior to each other in a multicriteria sense.

As shown in Figs. 1e–g, solutions from the experiments  $A_1$ ,  $B_1$ ,  $C_1$ , and  $C_3$  are superior to the default case; for the remaining, nonsuperior cases ( $A_2$ ,  $A_3$ ,  $B_2$ ,  $B_3$ , and  $C_2$ ), sensible heat flux is the only variable that has higher errors than in the default case. This indicates that the parameter estimations in the locally coupled environment are reasonably successful, considering that the model structure is not perfect and may unfavorably affect the results to a certain degree. Although some of the optimal parameter sets are not well constrained in some cases, as shown in Figs. 1a–d (e.g., case  $B_2$ ), very similar objective function values have been achieved within each group, reflecting, at least partially, the well-known “nonuniqueness” or “equifinality” functional behavior noted in many modeling studies wherein different parameter sets in the parameter space lead to very similar model responses (Franks and Beven 1997; Beven and Franks 1999). Generally speaking, with the inclusion of some atmospheric parameters, B and C cases have achieved much lower errors (except for sensible heat) than A cases, for which only land surface parameters are used.

In the A cases (Fig. 1e), including atmospheric variables in the parameter estimation procedure (cases  $A_2$  and  $A_3$ ) achieves lower errors of air temperature, but results in higher latent heat and sensible heat errors, while performances on the other three variables ( $T_g$ ,  $P_{cp}$ , and  $R_{net}$ ) remain almost the same; also, there is little difference between cases  $A_2$  and  $A_3$  for all six of the variables, which reflects the dominant influence of atmospheric forcing variables in the optimizing land surface parameters. In the B cases wherein only atmospheric parameters are optimized (Fig. 1f), reasonably low rmses have been achieved for all the six variables except for sensible heat; in addition, the results from the three different cases are very similar to each other, implying that the choice of error criteria has little influence if only atmospheric parameters are used for optimization. When both land surface and atmospheric parameters are used (C cases; Fig. 1g), little difference is observed between the three cases ( $C_1$ ,  $C_2$ , and  $C_3$ ) for four of the six variables ( $\lambda E$ ,  $T_g$ ,  $R_{net}$ , and  $T_a$ ). How-

ever, there is marked trade-off between the ability of the model to simultaneously reproduce both sensible heat and precipitation: the rmse for  $H$  is lowest in case  $C_1$  and highest in case  $C_2$ , while the reverse is true for the rmse of  $P_{cp}$ . This can also be noted for A cases and B cases, reflecting the trade-offs that can be detected by application of multicriteria methods, as has also been observed in other parameter estimation studies (e.g., Gupta et al. 1999). In general, case  $C_3$  (blue) appears to be preferable to all the other cases in that it achieves reasonably low errors for all the land surface and atmospheric fluxes/variables examined.

To examine the rmse improvements for each individual variable in comparison to the default case, the case-average rmses are shown as grouped bar graphs in Fig. 2 for each variable. The number shown in the title of each plot indicates the default rmse from a control run with the default parameters, and the values plotted on the bar graphs are normalized with respect to the corresponding default rmses. For each variable, the bars are grouped into A, B, and C cases, with white, gray, and black bars representing the first, second, and third cases, respectively. Similar to Figs. 1e–g, Fig. 2 shows that the rmses of the fluxes/variables after optimization are lower than the default for all variables except sensible heat. Further, including atmospheric parameters in the parameter estimation process helps to achieve lower errors. In general, the results are best for ground temperature, latent heat, and net radiation for which the rmse values are approximately 50% of the default case when atmospheric parameters are included in the optimization process. The results for sensible heat tend to be poor, especially in the second cases and B cases ( $A_2$ ,  $B_1$ ,  $B_2$ ,  $B_3$ , and  $C_2$ ), in which only atmospheric variables are used for error criteria and/or only atmospheric parameters are optimized. However, the lowest rmses of precipitation have been achieved in cases  $B_2$  and  $C_2$  with improvements of about 50%, while high precipitation errors tend to appear in the A cases, wherein only land surface parameters are optimized, and in case  $C_1$ , wherein only land surface variables are used for error criteria. The improvements in the rmse of air temperature are around 30% for all cases except  $A_1$ .

#### d. Time series

The most meaningful way to evaluate the performance of a numerical model is to examine its ability to satisfactorily reproduce the observed time series of important model outputs. Figure 3 presents a comparison between the observations and model simulations from a control run with the default parameters for the six variables: latent heat, sensible heat, ground temperature, precipitation, net radiation, and air temperature. The time series are shown on the left, with light and bold lines representing model simulations and observations, respectively, and the scatterplots are shown on the right, with  $x$  axes and  $y$  axes denoting the model-

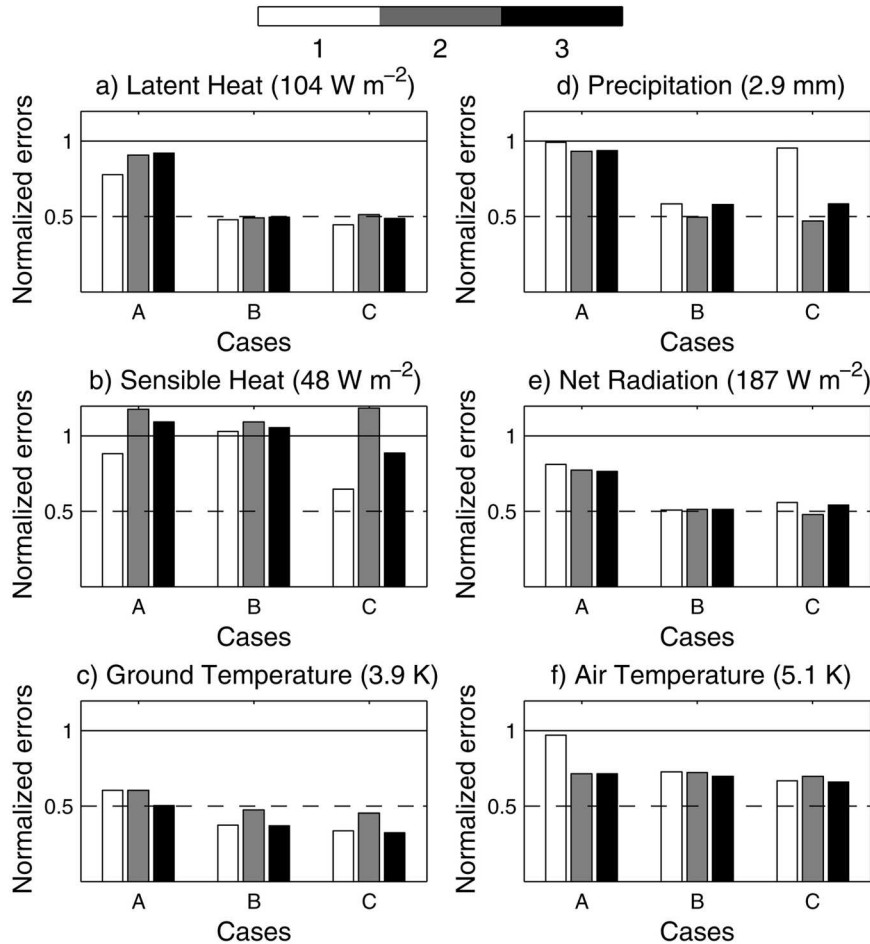


FIG. 2. Comparison of the case-average objective function values (rmses) scaled by the default rmses for (a) latent heat, (b) sensible heat, (c) ground temperature, (d) precipitation, (e) net radiation, and (f) air temperature. The value shown in the title of each plot is the corresponding default objective function value.

computed values and the observations, respectively. The rmse, correlation coefficient ( $R$ ), and bias of each variable are also shown above the corresponding plot. The time series and scatterplots in Fig. 3 show that the energy partition of model with default model parameters is incorrect: the model consistently overestimates latent heat and underestimates sensible heat; the model also considerably overestimates ground temperature, especially during the continuous raining period near the end of the simulation. On the atmospheric side, the model generates too frequent, and too weak, precipitation compared to the observation, and it overestimates net radiation and air temperature, especially near the end of the simulation period. The inability of the model to reproduce these time series, especially precipitation and air and ground temperatures, can be at least partially attributed to the deficiencies of the convection triggering function used in the SCCM, which has caused large thermal biases in the model simulations (Xie and Zhang 2000).

Considering the strong trade-off observed between precipitation and sensible heat flux, cases  $C_1$  and  $C_2$  are selected as representatives of “good” simulations for sensible heat and precipitation, respectively, and the time series are shown in Figs. 4 and 5. The gray shaded regions represent the modeled ranges corresponding to the entire set of solutions from case  $C_1$  or  $C_2$ , while in the scatterplots, the midpoints of the modeled ranges are used. As can be noted from Figs. 3 and 4, with the parameter estimates from case  $C_1$ , the model simulations match the land surface fluxes/variables ( $\lambda E$ ,  $H$ , and  $T_g$ ) much better than in the default case; although only land surface fluxes/variables are used in case  $C_1$  for error criteria, the model also performs better on the simulations of net radiation and air temperature, indicating the significant influence of land-atmosphere interactions. There is, however, no visually detectable improvement in the simulation of precipitation, except that the bias is considerably reduced from 2.1 mm in the default case to 0.8 mm in case  $C_1$ . In case  $C_2$  (Fig. 5),

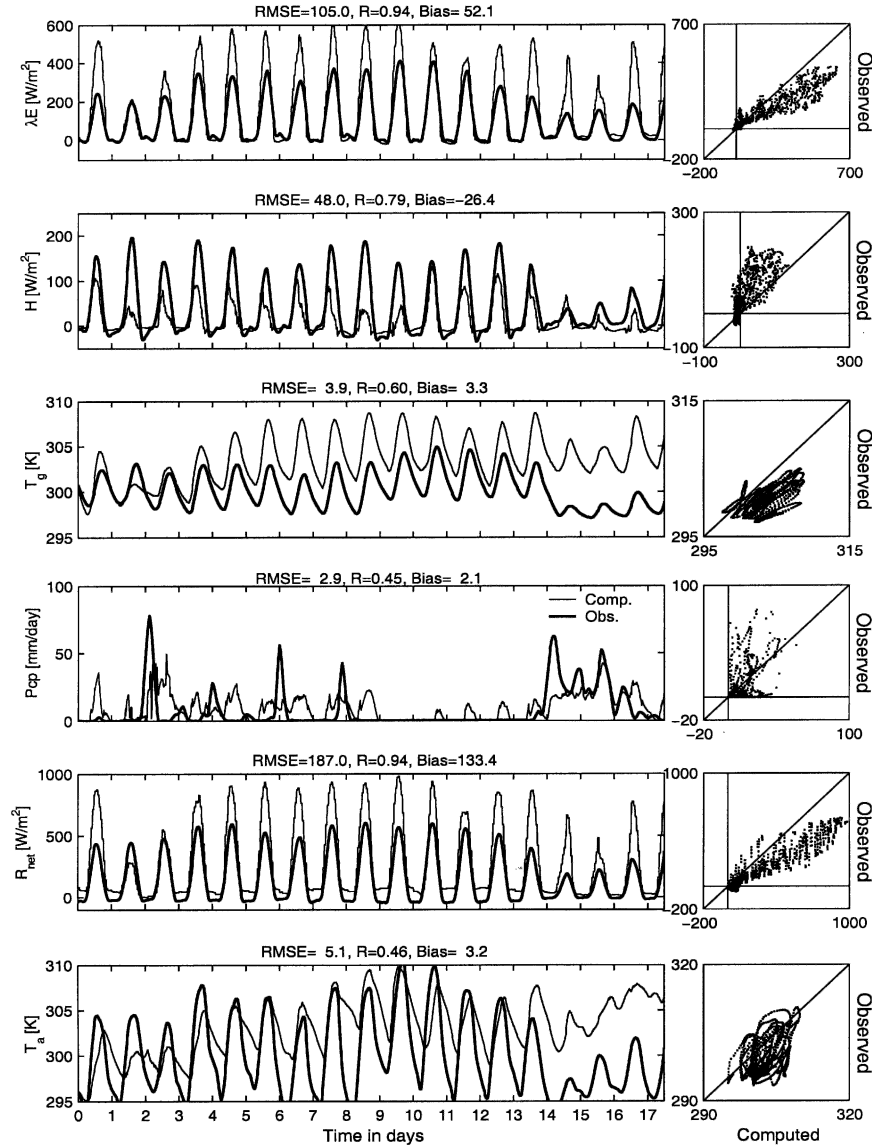


FIG. 3. Comparison of modeled variables (light line) in the control run with the observed data (bold line). The time series are shown on the left while the scatterplots are shown on the right. The rmse, correlation coefficient, and bias for each variable are also listed above each plot.

wherein only atmospheric variables ( $Pcp$ ,  $R_{net}$ , and  $T_a$ ) are used for error criteria, the model-simulated precipitation has been significantly improved ( $rmse = 1.5$  mm,  $R = 0.86$  mm,  $bias = 0.6$  mm), matching the major observed rainfall events of the simulation period; the model also provides reasonably better matching of the diurnal pattern of variability in the observed net radiation compared to case  $C_1$ . These, however, are at the expense of significantly poorer matching of the sensible heat flux, slightly poorer matching of the latent heat flux, and somewhat deteriorated performance on ground and air temperatures for which the amplitude of diurnal variations are too small to be realistic.

## 5. Stepwise parameter estimations

Considering that optimizing both land surface parameters and atmospheric parameters simultaneously in the coupled environment may make the parameter estimation process cumbersome and computationally expensive, three further cases ( $D_1$ ,  $D_2$ , and  $D_3$ ; Table 3) were also established to conduct the parameter estimation in a two-step manner. In these cases, the land surface parameters were optimized first in an offline mode using the LSM to obtain a set of optimal land surface parameters ( $\{\theta^{opt}\}$ ; Table 1, last column); the atmospheric parameters ( $\{\phi\}$ ) were then optimized in the

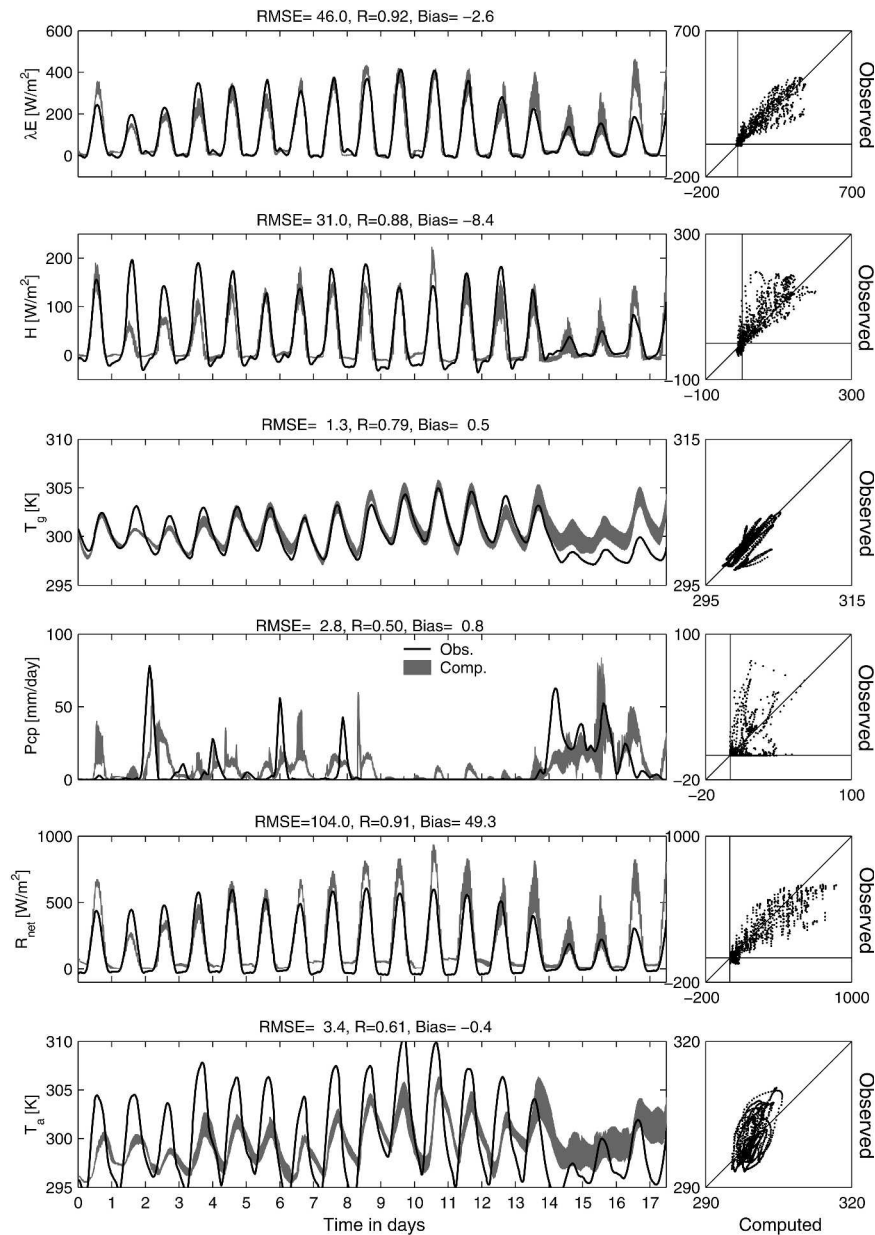


FIG. 4. Comparison of modeled variables (lightly shaded region) with the observed data (bold line) for the parameter sets estimated by case  $C_1$ . The time series on the left show the modeled ranges corresponding to the entire Pareto solution set while the scatterplots on the right compare the midpoints of the modeled ranges with the observations.

locally coupled environment using the SCCM, with the land surface parameter set  $\{\theta\}$  fixed at  $\{\theta^{off}\}$ . Because the land surface parameters and the atmospheric parameters were successively optimized in an offline mode and a coupled mode, respectively, these cases are referred to as stepwise cases, in contrast to the corresponding single-step cases  $C_1$ ,  $C_2$ , and  $C_3$ .

Because of the highly sophisticated numerical computations involved in atmospheric modeling, coupled simulations usually require much more computational

time than offline simulations (8 s for a single coupled run and less than 1 s for a single offline run in this case). Also, with all land parameters estimated offline, optimization of only a small amount of atmospheric parameters (eight in this case) in the coupled mode needs much less function evaluations to satisfy a prescribed convergence criterion. Hence, a stepwise scheme can save a significant amount of computational time compared to a corresponding single-step scheme (about 50% or 24 h in this case). Accordingly, it is of interest

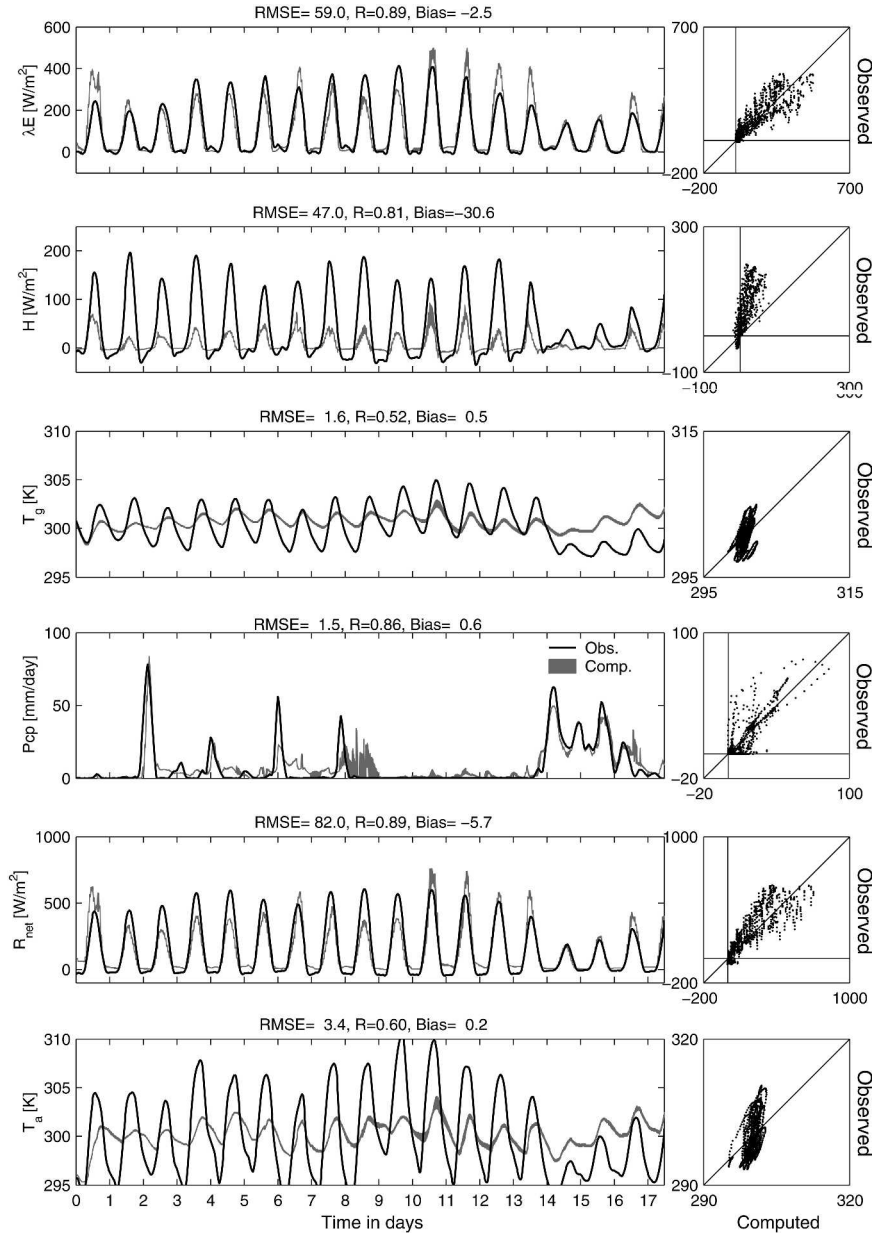


FIG. 5. Same as Fig. 4 but for case C<sub>2</sub>.

to examine whether the results from the stepwise cases are comparable to those from the single-step cases. Shown in Fig. 6 are the optimal parameter sets obtained in the D cases compared to those from the corresponding C cases for the land surface (Figs. 6a–c) and the atmosphere (Figs. 6d–f). It can be noted that the land surface parameter set  $\{\theta^{off}\}$  used in the D cases is different from those obtained through coupled procedures in cases C<sub>1</sub>, C<sub>2</sub>, and C<sub>3</sub>, which is not surprising, considering that the model-generated atmospheric forcing in the coupled system is quite different from the observations used for the offline calibration. This also indicates that the land–atmosphere interactions can have consid-

TABLE 3. The stepwise cases.

Case	Evaluation variables	Land surface parameters ( $\theta$ )	Atmospheric parameters ( $\phi$ )
D Cases	D <sub>1</sub> $\lambda E, H, T_g$ D <sub>2</sub> $Pcp, R_{net}, T_a$ D <sub>3</sub> $\lambda E, H, T_g, Pcp, R_{net}, T_a$	$\{\theta^{off}\}$ *	Optimized

\*  $\theta^{off}$ : An optimal land surface parameter set from offline LSM calibration.

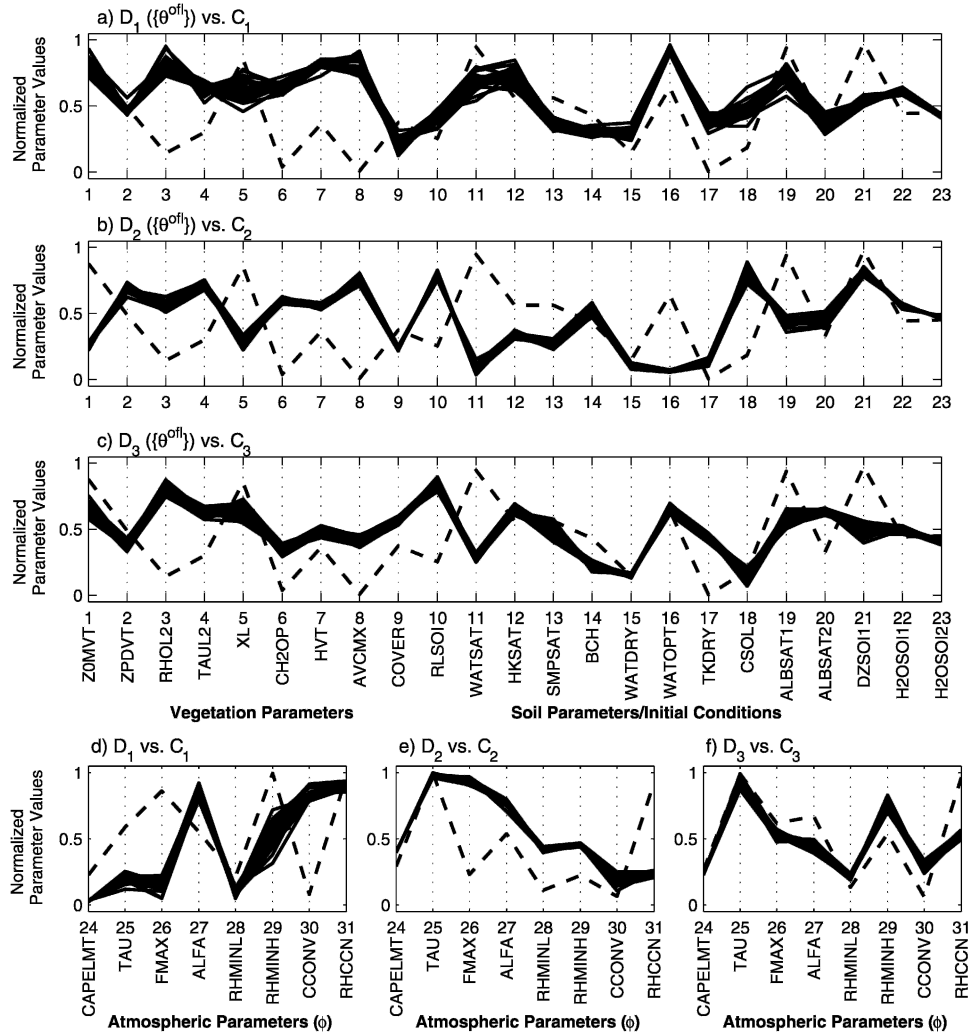


FIG. 6. Comparison of the solutions from the stepwise cases ( $D_1$ ,  $D_2$ , and  $D_3$ ) with those from the corresponding single-step cases ( $C_1$ ,  $C_2$ , and  $C_3$ ) for land surface parameters: (a)  $D_1$  vs  $C_1$ , (b)  $D_2$  vs  $C_2$ , (c)  $D_3$  vs  $C_3$ , and atmospheric parameters: (d)  $D_1$  vs  $C_1$ , (e)  $D_2$  vs  $C_2$ , and (f)  $D_3$  vs  $C_3$ . For the  $C$  cases, the entire Pareto set of solutions are shown (solid line), while for the  $D$  cases, only the midpoints of the solution set are shown (dashed line).

erable influences on the estimation of land surface parameters. Figures 6a–c also show that the land surface parameter sets from case  $C_1$  are less different from  $\{\theta^{off}\}$  than those from cases  $C_2$  and  $C_3$  (especially case  $C_2$ ). This can be attributed to the fact that, in case  $C_1$  and the offline case, only land surface fluxes/variables ( $\lambda E$ ,  $H$ , and  $T_g$ ) were used for error criteria, while in the other two cases some atmospheric variables were used either instead of ( $C_2$ ) or together with the land surface fluxes/variables ( $C_3$ ). Further, Fig. 6a shows that the land–atmosphere interactions seem to have less effect on the estimation of soil parameters than that of vegetation parameters: 5 out of 9 vegetation parameters (RHOL2, TAUL2, CH2OP, HVT, and AVCMX), compared to 2 out of 14 for soil parameters (TKDRY and DZSOI1), have markedly distinct optimal values

offline and coupled calibrations. This can be at least partially related to the considerable biases in the model-generated precipitation (Xie and Zhang, 2000), which mostly affect vegetation–atmosphere interactions rather than direct soil–air flux exchanges since the surface is highly vegetated (vegetation cover fraction = 85%). Given that the land surface parameters are different in  $C$  and  $D$  cases, it would be interesting to examine how this affects the estimation of the atmospheric parameters. Because the atmospheric parameters are well constrained in all  $D$  cases, the midpoints rather than the entire set of solutions are plotted for the  $D$  cases (Figs. 6d–f). As can be noted, most of the atmospheric parameters estimated by case  $D_1$  are different from those in case  $C_1$ . The same is true for case  $D_2$  and  $C_2$ ; cases  $C_3$  and  $D_3$ , however, have resulted in very

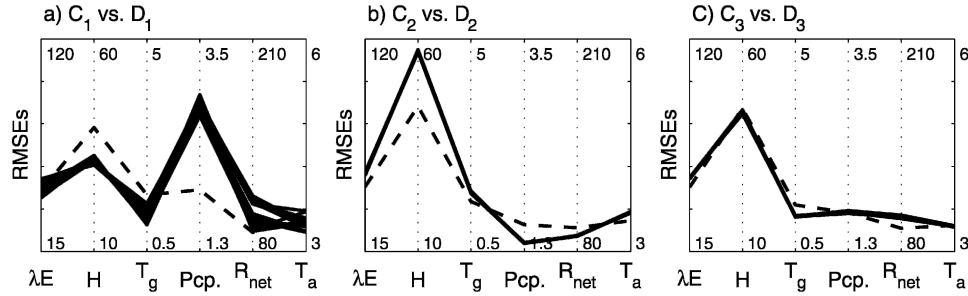


FIG. 7. Same as Figs. 6a–c (or Figs. 6d–f) but for the objective function values.

similar estimations of atmospheric parameters, except that there is a distinction between the values of RHCCN in the two cases. The ranges of the atmospheric parameter estimates obtained in case  $D_3$  are also presented in Table 1 (lower-right corner), in which it can be noted that the atmospheric parameter estimates in this case are well constrained but considerably different from the a priori values.

For the corresponding objective function values, Fig. 7 shows that cases  $C_1$  and  $D_1$  have resulted in different rmse for sensible heat and precipitation, and the same is true for cases  $C_2$  and  $D_2$ ; the other four variables ( $\lambda E$ ,  $T_g$ ,  $R_{net}$ , and  $T_a$ ), however, have very close error values in cases  $C_1$  and  $D_1$ , and also in cases  $C_2$  and  $D_2$ . This implies that the differences between the land surface and atmospheric parameters in cases  $C_1$  and  $D_1$  (or cases  $C_2$  and  $D_2$ ) tend to only affect the model simulations of sensible heat and precipitation, which are the two variables that the model is unable to simulate well simultaneously, as noted from the single-step cases presented in section 4. From the multicriteria point of view, cases  $D_1$  and  $D_2$  are preferable to cases  $C_1$  and  $C_2$  in that the former can provide reasonable performances on all six variables. It is most interesting to note that the rmse achieved in cases  $D_3$  and  $C_3$  are almost identical, indicating that the atmospheric parameters have a dominant influence on the simulations of a coupled model. The equivalent performances of cases  $D_3$  and  $C_3$  can be further confirmed by the very close time series simulated in these two cases for all the six variables, as shown in Fig. 8, wherein it can be noted that the time series from the two cases are highly correlated ( $R > 0.95$ ) except for ground temperature.

## 6. Summary and conclusions

Over the last two decades, substantial research has been devoted to the estimation of parameters of hydrological and land surface models in an offline mode, while little or no attention has been paid to issues of parameter estimation in a coupled mode. The latter is, however, more relevant in the context of parameterization evaluations for coupled land–atmosphere models, a major interest of the Global Land–Atmosphere Sys-

tem Study (GLASS). The study presented here was motivated by the need to identify feasible and effective approaches to estimating parameters for coupled land–atmosphere models that can enable them to provide relatively unbiased simulations of important fluxes and state variables. Several schemes were tested using the locally coupled NCAR SCCM to explore the effects of including atmospheric parameters and forcing variables in the optimization process to help constrain parameter and simulation uncertainties. The value of performing parameter estimation for a coupled model in a stepwise manner was also investigated.

Overall, all the schemes tend to provide well-constrained “optimal” parameter sets and reasonably low objective function values. In the coupled environment, the inclusion of atmospheric variables for error criteria helps to better constrain the land surface parameters, while the inclusion of land surface fluxes/variables tends to better constrain the atmospheric parameters, illustrating the influence of “driving” variables on the optimization results. Consequently, the use of both land surface and atmospheric variables as error criteria can help to achieve reasonably well-constrained solutions for both land surface and atmospheric parameters of a coupled model. In terms of objective function values and time series, the model generally performs better with optimal parameters than with the default parameters, indicating the feasibility and success of parameter estimations in the locally coupled environment. In particular, the results tend to be best for ground temperature, latent heat, and net radiation, and worst for sensible heat. Also, there is a noticeable trade-off in the ability of the model to simultaneously reproduce both observed sensible heat flux and precipitation, making it necessary to explicitly include these two terms as optimization criteria to achieve acceptable simulations. When the atmospheric parameters are included in the optimization process, the resulting rmse (except those of sensible heat) are better than when only land surface parameters are used. This is consistent with the results from the sensitivity analysis study of Liu et al. (2004), which found the coupled model to be highly sensitive to changes in these atmospheric parameters. Accordingly, for a coupled land–atmosphere

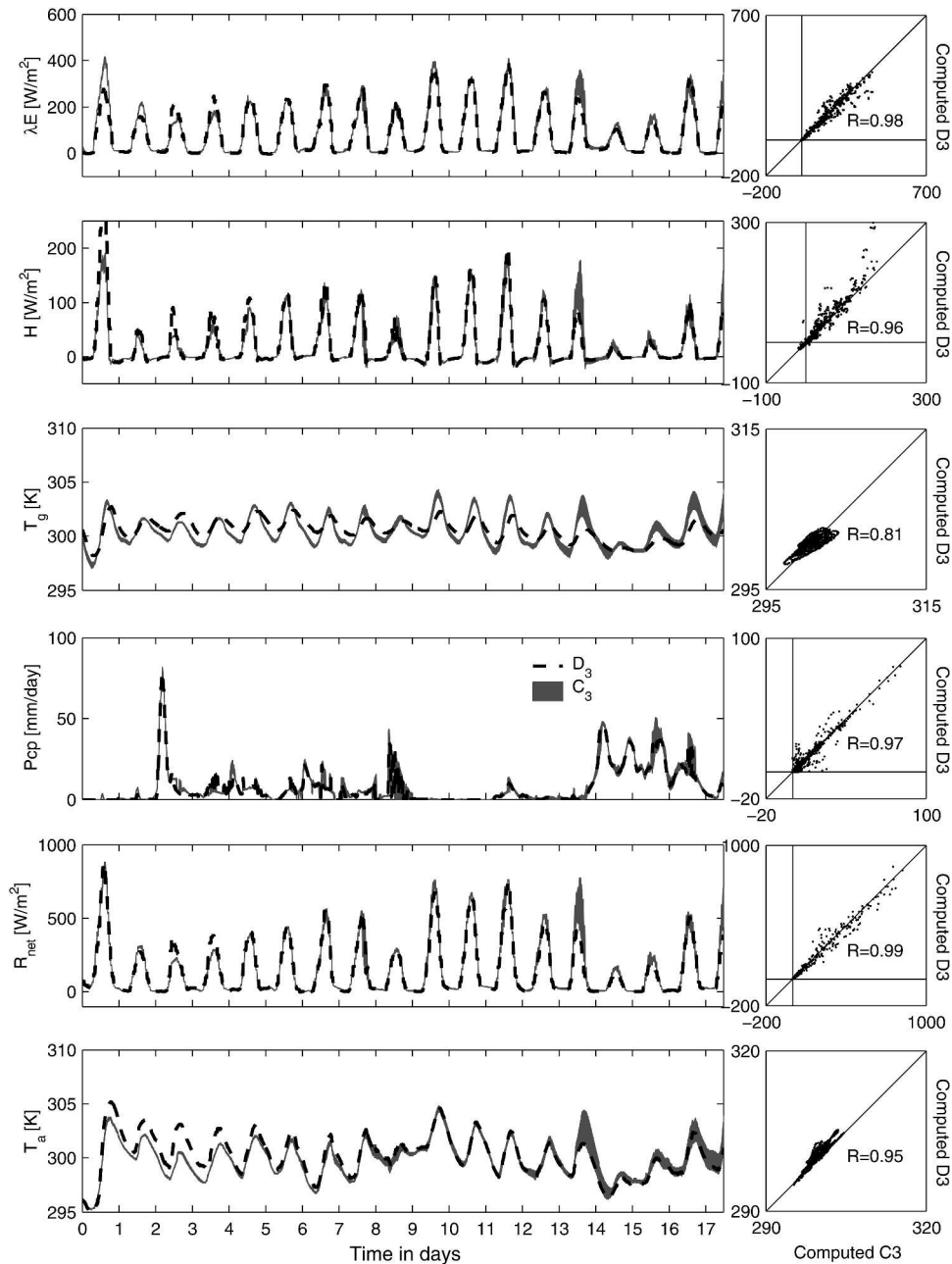


FIG. 8. Comparison of time series and scatterplots for cases  $C_3$  and  $D_3$ . For case  $C_3$ , the modeled ranges corresponding to the entire Pareto solution set are shown for the time series (lightly shaded region), while only the midpoints of the model ranges are shown for case  $D_3$  (dashed line). Scatterplots correspond to the midpoints for both cases.

model, it is desirable to optimize both land surface and atmospheric parameters simultaneously and use both land surface and atmospheric fluxes/variables as optimization criteria for parameter estimation. The results from this study also show that it is practical to optimize the land surface and atmospheric parameters successively in offline and coupled modes, respectively, considering that this stepwise scheme can achieve solutions

comparable to the corresponding single-step cases but with much less difficulty and computational time. A stepwise scheme, although preventing the exploration of the full land-atmosphere parameter space, can also avoid any negative impacts that biases in model-generated atmospheric forcing may have on the effectiveness of the optimal values of the land parameters.

Regardless of the site and model-specific tendency of

the optimal parameter values retrieved via parameter estimation, this study has demonstrated a feasible and effective, general framework for constraining the parameters of a locally coupled model using observational data, thereby facilitating the broader problem of testing alternative land surface parameterizations in a coupled mode. With the availability of high-power computation resources (e.g., multiprocessor clusters) and an efficient parallelized software system, this parameter estimation framework can be extended to applications over larger domains (e.g., regional scales) within an affordable time frame. It is worth mentioning that the weighting method, which has facilitated the application of SCE-UA to multiobjective parameter estimation in this study, tends to ignore the impacts of model structural deficiencies on reproducing each individual flux/variable. Hence, in future follow-up research it is worthwhile to explore the application of the multiobjective conditioning methodology suggested by Franks et al. (1999), in which error variances were normalized by their corresponding minimum values to reduce effects of structural deficiencies.

*Acknowledgments.* This study was primarily supported by SAHRA (an NSF Center for Sustainability of Semi-Arid Hydrology and Riparian Areas) under Grant EAR-9876800. Additional support came from NASA EOS Grants NAG5-3640-5 and NAG8-1531. The National Center for Atmospheric Research (NCAR) is thanked for publishing the model codes and datasets online. Special thanks are due to Drs. Brian Cosgrove and Andy Pitman for comments and to Dr. Jiming Jin for assistance in determining the parameter boundaries.

#### REFERENCES

- Beven, K. J., and S. W. Franks, 1999: Functional similarity in landscape scale SVAT modeling. *Hydrol. Earth Syst. Sci.*, **3** (1), 85–93.
- Bonan, G. B., 1995a: Land–atmosphere CO<sub>2</sub> exchange simulated by a land surface process model coupled to an atmospheric general circulation model. *J. Geophys. Res.*, **100**, 2817–2831.
- , 1995b: Sensitivity of a GCM simulation to inclusion of inland water surfaces. *J. Climate*, **8**, 2691–2704.
- , 1996: A land surface model (LSM version 1.0) for ecological, hydrological, and atmospheric studies: Technical description and user's guide. NCAR Tech. Note NCAR/TN-417+STR, National Center for Atmospheric Research, Boulder, CO, 150 pp.
- , 1997: Effects of land use on the climate of the United States. *Climate Change*, **37**, 449–486.
- , 1999: Frost followed the plow: Impacts of deforestation on the climate of the United States. *Ecol. Appl.*, **9**, 1305–1315.
- , K. J. Davis, D. Baldocchi, D. Fitzjarrald, and H. Neumann, 1997: Comparison of the NCAR LSM1 land surface model with BOREAS aspen and jack pine tower fluxes. *J. Geophys. Res.*, **102**, 29 065–29 075.
- Burnash, R. J. E., R. L. Ferral, and R. A. McGuire, 1973: A generalized streamflow simulation system. Joint Federal–State River Forecast Center Rep., Sacramento, CA, 204 pp.
- Cosgrove, B. A., and Coauthors, 2003: Real-time and retrospective forcing in the North American Land Data Assimilation System (NLDAS) project. *J. Geophys. Res.*, **108**, 8842, doi:10.1029/2002JD003118.
- Craig, S. G., K. J. Holmen, G. B. Bonan, and P. J. Rasch, 1998: Atmospheric CO<sub>2</sub> simulated by the National Center for Atmospheric Research Community Climate Model. 1. Mean fields and seasonal cycles. *J. Geophys. Res.*, **103**, 13 213–13 235.
- Desborough, C. E., 1999: Surface energy balance complexity in GCM land surface models. *Climate Dyn.*, **15**, 389–403.
- Dickinson, R. E., A. Henderson-Sellers, P. J. Kennedy, and M. F. Wilson, 1986: Biosphere Atmosphere Transfer Scheme (BATS) for the NCAR Community Climate Model. NCAR Tech. Note NCAR/TN275+STR, 69 pp.
- , —, and —, 1993: Biosphere–atmosphere transfer scheme (BATS) version 1e as coupled to the NCAR community climate model. NCAR Tech. Note NCAR/TN-387+STR, 72 pp.
- Dirmeyer, P. A., A. J. Dolman, and N. Sato, 1999: The global soil wetness project: A pilot project for global land surface modeling and validation. *Bull. Amer. Meteor. Soc.*, **80**, 851–878.
- Dolman, A. J., and D. Gregory, 1992: Assessing the sensitivity of a land surface scheme to parameters used in tropical deforestation experiments. *Quart. J. Roy. Meteor. Soc.*, **118**, 1101–1116.
- Duan, Q. Y., V. K. Gupta, and S. Sorooshian, 1992: Effective and efficient global optimization for conceptual rainfall-runoff models. *Water Resour. Res.*, **28**, 1015–1031.
- Franks, S. W., and K. J. Beven, 1997: Bayesian estimation of uncertainty in land surface–atmosphere flux predictions. *J. Geophys. Res.*, **102** (D20), 23 991–23 999.
- , —, and J. H. C. Gash, 1999: Multi-objective conditioning of a simple SVAT model. *Hydrol. Earth Syst. Sci.*, **3**, 477–489.
- Goldberg, D. E., 1989: *Genetic Algorithms in Search, Optimization, and Machine Learning*. Addison-Wesley, 412 pp.
- Gupta, H. V., S. Sorooshian, and P. O. Yapo, 1998: Toward improved calibration of hydrological models: Multiple and non-commensurable measures of information. *Water Resour. Res.*, **34**, 751–763.
- , L. A. Bastidas, S. Sorooshian, W. J. Shuttleworth, and Z. L. Yang, 1999: Parameter estimation of a land surface scheme using multi-criteria methods. *J. Geophys. Res.*, **104** (D16), 19 491–19 504.
- Gupta, V. K., and S. Sorooshian, 1985: The relationship between data and the precision of parameter estimates of hydrological models. *J. Hydrol. Amsterdam*, **81**, 57–77.
- Hack, J. J., J. A. Pedretti, and J. C. Petch, cited 1999: SCCM user's guide, version 1.2. [Available online at <http://www.cgd.ucar.edu/cms/scem/scem.html>.]
- Henderson-Sellers, A., A. J. Pitman, P. K. Love, P. Irannejad, and T. H. Chen, 1995: The Project for Intercomparison of Land Surface Parameterization Schemes (PILPS): Phases 2 and 3. *Bull. Amer. Meteor. Soc.*, **76**, 489–503.
- Kiehl, J. T., J. J. Hack, G. B. Bonan, B. A. Boville, B. P. Briegleb, D. L. Williamson, and P. J. Rasch, 1996: Description of the NCAR Community Climate Model (CCM3). NCAR Tech. Note NCAR/TN-420+STR, 151 pp.
- Koster, R. D., and P. S. Eagleson, 1990: A one-dimensional interactive soil–atmosphere model for testing formulations of surface hydrology. *J. Climate*, **3**, 593–606.
- Leavesley, G. H., R. W. Lichty, B. M. Troutman, and L. G. Saindon, 1983: Precipitation-runoff modeling system: User's manual. Water Resources Investigative Rep. 83-4238, U.S. Geological Survey, Denver, CO, 207 pp.
- Lettenmaier, D., D. Lohmann, E. F. Wood, and X. Liang, 1996: PIPLS-2c workshop report. Princeton University, Princeton, NJ, 10, 28–31.
- Liu, Y., L. A. Bastidas, H. V. Gupta, and S. Sorooshian, 2003: Impacts of a parameterization deficiency on off-line and coupled land-surface model simulations. *J. Hydrometeorol.*, **4**, 901–914.

- , H. V. Gupta, S. Sorooshian, L. A. Bastidas, and J. W. Shuttleworth, 2004: Exploring parameter sensitivities of the land surface using a locally coupled land–atmosphere model. *J. Geophys. Res.*, **109**, D21101, doi:10.1029/2004JD004730.
- Lynch, A. H., G. B. Bonan, F. S. Chapin III, and W. Wu, 1999: The impact of tundra ecosystems on the surface energy budget and climate of Alaska. *J. Geophys. Res.*, **104** (D6), 6647–6660.
- , S. McIlwaine, J. Beringer, and G. B. Bonan, 2001: An investigation of the sensitivity of a land surface model to climate change using a reduced form mode. *Climate Dyn.*, **17**, 643–652.
- Pitman, A. J., Z.-L. Yang, and A. Henderson-Sellers, 1993: Sub-grid scale precipitation in AGCMs: Re-assessing the land surface sensitivity using a single column model. *Climate Dyn.*, **9**, 33–41.
- Randall, D. A., and D. G. Cripe, 1999: Alternative methods for specification of observed forcing in single-column models and cloud system models. *J. Geophys. Res.*, **104** (D20), 24 527–24 545.
- , K.-M. Xu, R. J. C. Somerville, and S. Iacobellis, 1996: Single-column models and cloud ensemble models as links between observations and climate models. *J. Climate*, **9**, 1683–1697.
- Rodell, M., and Coauthors, 2004: The Global Land Data Assimilation System. *Bull. Amer. Meteor. Soc.*, **85**, 381–394.
- Sellers, P. J., Y. Mintz, and A. Dalcher, 1986: A simple biosphere model (SiB) for use within general circulation models. *J. Atmos. Sci.*, **43**, 505–531.
- , W. J. Shuttleworth, J. L. Dorman, A. Dalcher, and J. A. Roberts, 1989: Calibrating the simple biosphere model (SiB) for Amazonian tropical forest using field and remote sensing data. Part I: Average calibration with field data. *J. Appl. Meteor.*, **28**, 727–759.
- Sen, O. L., L. A. Bastidas, W. J. Shuttleworth, Z. L. Yang, H. V. Gupta, and S. Sorooshian, 2001: Impact of field calibrated vegetation parameters on GCM climate simulations. *Quart. J. Roy. Meteor. Soc.*, **127**, 1199–1224.
- Somerville, R. C. J., and S. F. Iacobellis, 1999: Single-column models, ARM observations, and GCM cloud-radiation schemes. *Phys. Chem. Earth*, **24B**, 733–740.
- Sorooshian, S., Q. Duan, and V. K. Gupta, 1993: Calibration of rainfall-runoff models: Application of global optimization to the Sacramento soil moisture accounting model. *Water Resour. Res.*, **29**, 1185–1194.
- Xia, Y., A. J. Pitman, H. V. Gupta, M. Leplastrier, A. Henderson-Sellers, and L. A. Bastidas, 2002: Calibrating a land surface model of varying complexity using multicriteria methods and the Cabauw dataset. *J. Hydrometeor.*, **3**, 181–194.
- Xie, S. C., and M. H. Zhang, 2000: Impact of the convection triggering function on single-column model simulations. *J. Geophys. Res.*, **105** (D11), 14 983–14 996.
- Xu, K.-M., and A. Arakawa, 1992: Semi-prognostic tests of the Arakawa–Schbert cumulus parameterization using simulated data. *J. Atmos. Sci.*, **49**, 2421–2436.
- Yan, J., and C. T. Haan, 1991: Multiobjective parameter estimation for hydrological models—Weighting of errors. *Trans. Amer. Soc. Agric. Eng.*, **34**, 135–141.
- Yapo, P. O., H. V. Gupta, and S. Sorooshian, 1998: Multi-objective global optimization for hydrological models. *J. Hydrol.*, **204**, 83–97.
- Zhang, M. H., and J. L. Lin, 1997: Constrained variational analysis of sounding data based on column-integrated conservations of mass, heat, moisture, and momentum: Approach and application to ARM measurements. *J. Atmos. Sci.*, **54**, 1503–1524.
- , —, R. T. Cederwall, J. J. Yio, and S. C. Xie, 2001: Objective analysis of ARM IOP data: Method and sensitivity. *Mon. Wea. Rev.*, **129**, 295–311.